Supporting Information

Enhancing Ag-alloyed Cu_2ZnSnS_4 solar cell performance by interfacial modification via In and Al

*Ping Fan, Yang He, Guangxing Liang, Zhigao Xie, Zixuan Yu, Jinhong Lin, Shuo Chen, Zhuanghao Zheng, Jingting Luo, and Zhenghua Su**

Shenzhen Key Laboratory of Advanced Thin Films and Applications, Key Laboratory of Optoelectronic Devices and Systems, College of Physics and Optoelectronic Engineering, Shenzhen University, Shenzhen, 518060, P. R. China
E-mail: zhsu@szu.edu.cn

Table S1 Device characteristics of CZTS solar cells with different Ag dopant (0%~7%).

Devices	PCE [%]	V_{OC} [mV]	FF [%]	J_{SC} [mA/cm^2]	E_g [eV]
Device-Ag0	6.4	640	59	16.9	1.50
Device-Ag1	7.0	662	62	17.1	1.50
Device-Ag3	7.6	671	64	17.5	1.50
Device-Ag5	7.3	676	63	17.1	1.51
Device-Ag7	5.7	681	51	16.5	1.53

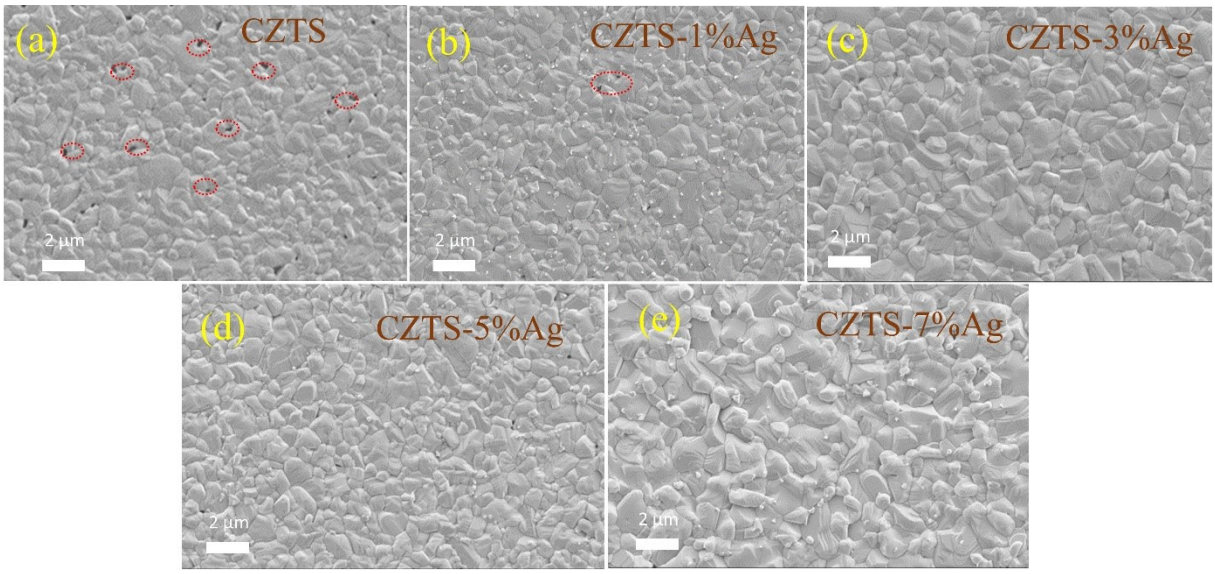

Fig. S1 (a) ~ (e) Surface SEM images for CZTS thin films with different Ag doping.

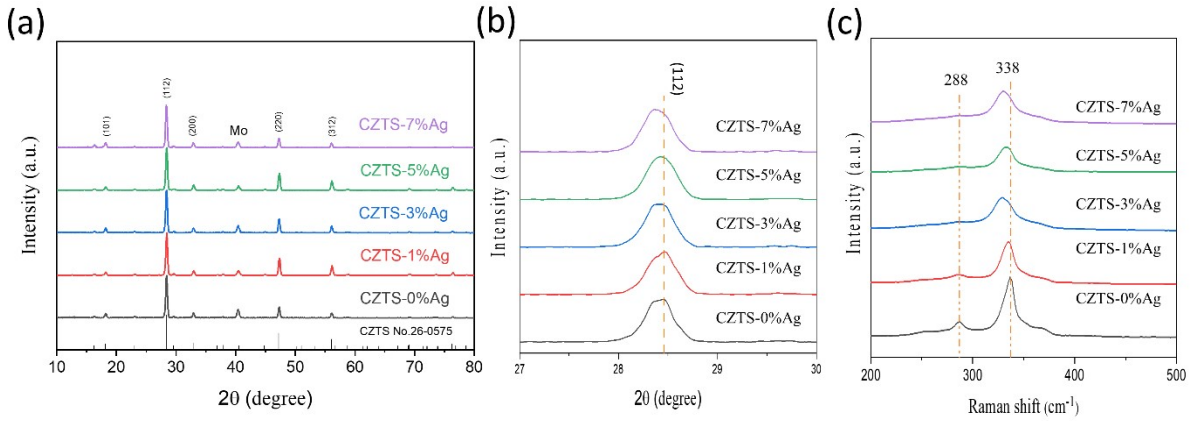

Fig. S2 (a) XRD patterns for CZTS thin films with different Ag doping (b) Magnified region from 27–30 degree from XRD patterns (c) Raman spectra for CZTS thin films with different Ag doping.

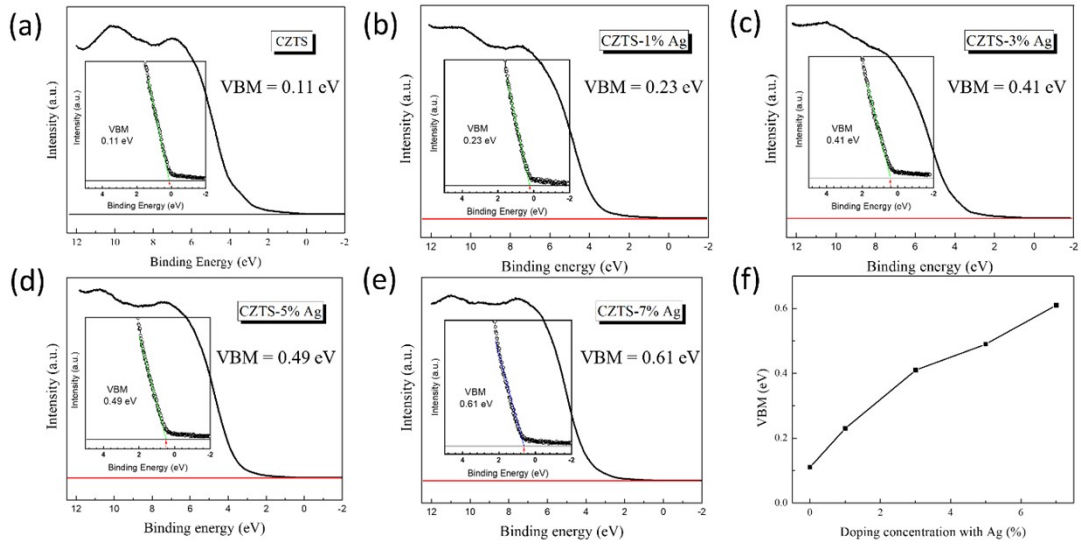

Fig. S3 (a~f) UPS valence band data for CZTS thin films with different Ag doping concentration (0% ~ 7%). The inset pictures show the linear extrapolations for UPS data closed to valence band maximum.

Temperature dependent capacity frequency (CF-T) spectrum

The capacity frequency (CF-T) spectrum (AS) of CZTS solar cells in the temperature range of 110–300 k are shown in Figure S4 and S5, and the corresponding Arrhenius plot for the inflection points in the AS is shown in Figure S6. The inflection point frequency ω_0 for each AS curve is determined by using the maximum point of $\omega dC/d\omega$ vs. ω plots. The fitting of the Arrhenius plot is given according to Equation 1.

$$\omega_0 = 2\pi v_0 T^2 \exp\left(\frac{-E_a}{\kappa T}\right) \quad (1)$$

where k is the Boltzmann constant, ω_0 is the step frequency, v_0 is the average escaping frequency of the traps, E_a is the energy depth of the defect relative to the valence band maximum, which represents the average defect energy level in the band gap.

To obtain the energetic defect distribution for CZTS devices, the frequencies in CF scanning are converted into energies for x-axis using Equation 2 and differentiated capacitance spectra at each temperature is superimposed using Equation 3.

$$\mathrm{E}(\omega) = \mathrm{K}_B T \ln\left(\frac{2\pi v_0 T^2}{\omega}\right) \quad (2)$$

$$N_t(E(\omega)) = -\frac{V_d}{qWkT}.\omega\frac{dC}{d\omega}. \quad (3)$$

where V_d is built in potential and W is depletion width, which are extracted from Capacitance-Voltage measurement.

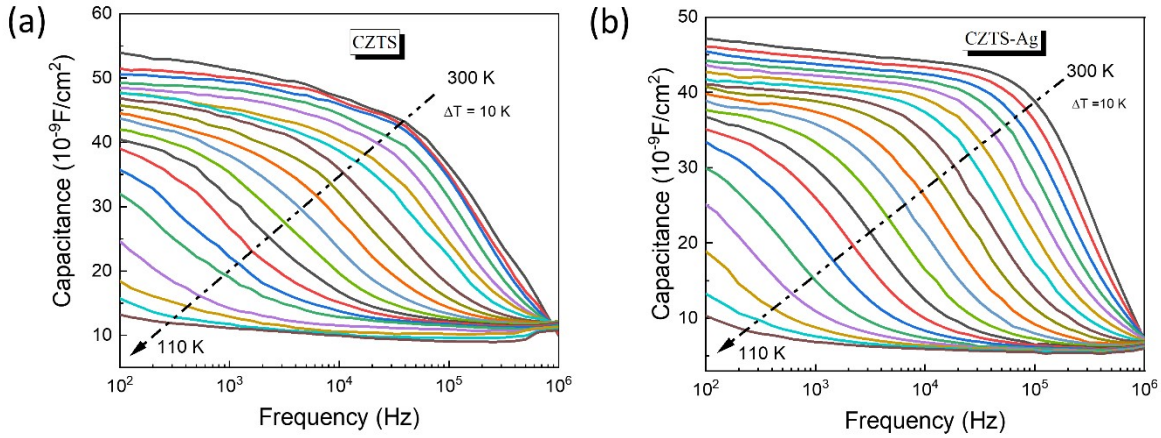

Fig. S4 Admittance spectra of CZTS devices without Ag doping (a) and with 3% Ag doping (b), measured at temperature between 110 K and 300 K with a step of 10 K.

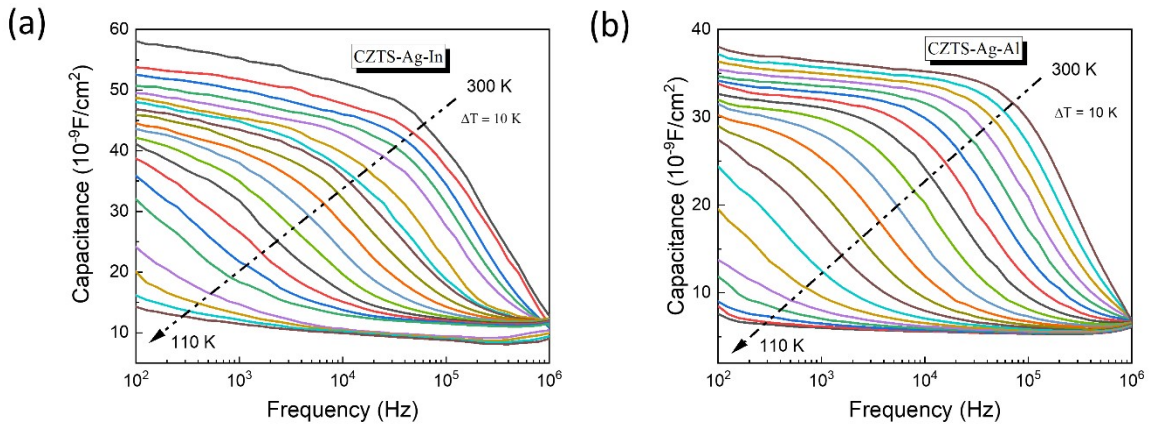

Fig. S5 Admittance spectra of CZTS-Ag devices with In (a) and Al (b) interface doping, measured at temperature between 110 K and 300 K with a step of 10 K.

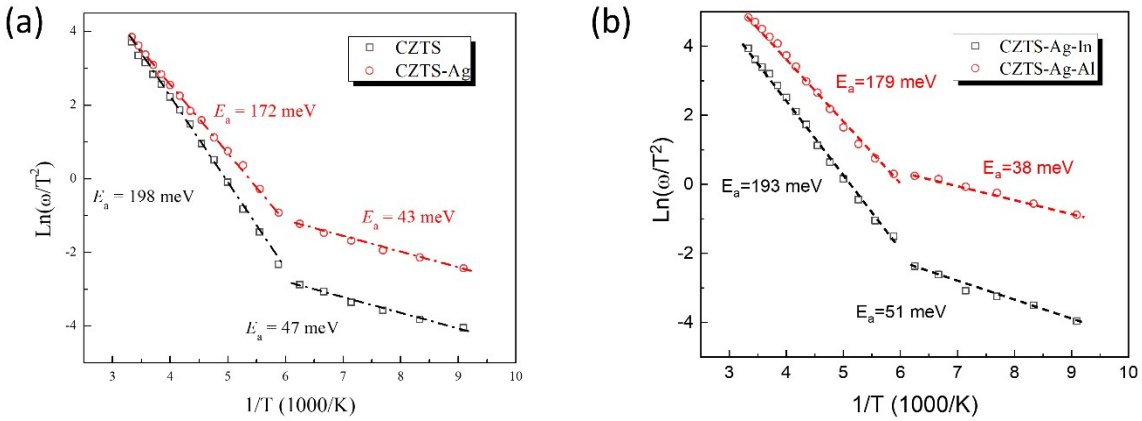

Fig. S6 Arrhenius plot of the inflection frequencies determined from the derivative of the admittance spectra for (a) CZTS devices without and with 3% Ag doping (b) CAZTS devices with In and Al interface doping.

Band alignment

The CBO can be estimated by CBO = $(E_{gap}^{b} - E_{gap}^{a}) + (E_{VB}^{b} - E_{VB}^{a}) + V_{bb}$, where E_{VB}^{b} and E_{VB}^{a} are the energy positions of the valence band edge of bulk CdS and bulk CZTS, while V_{bb} is the band bending, which can be obtained by the formula:

$V_{bb} = (E_{CL}^{a} - E_{CL}^{a}(i)) + (E_{CL}^{b}(i) - E_{CL}^{b})$, where E_{CL}^{a} and E_{CL}^{b} represent the core level energies of two elements in CZTS and CdS respectively, while $E_{CL}^{a}(i)$ and $E_{CL}^{b}(i)$ are the corresponding core level energies measured at the interface. In CZTS the elements of Cu, Zn and Sn were chosen and in CdS the element was Cd. Fig. S7 shows the band

bending values at different depth of CdS/CZTS interface for four CdS/CZTS heterojunctions with different doping. The binding energies of Cd 3d5/2 from CdS and Cu 2p3/2, Zn 2p3/2 and Sn 3d5/2 form CZTS were used. The calculated CBO values for four CdS/CZTS heterojunctions were shown in Table S2.

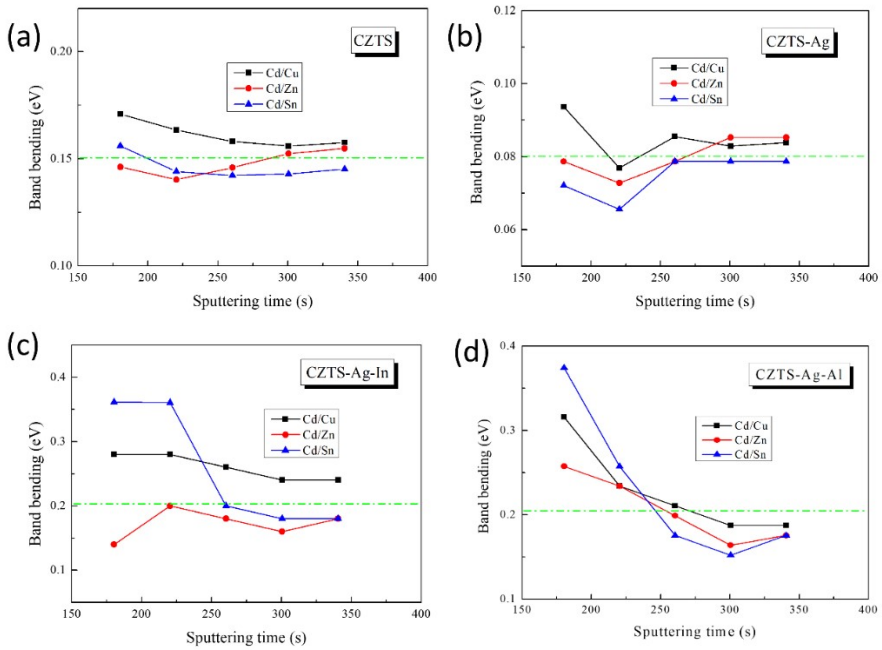

Fig. S7 The band bending values (3 data sets) as function of sputtering time for (a) pure CZTS (b) CZTS with 3% Ag doping (c) CZTS-Ag with In-doping and (d) CZTS-Ag with Al-doping.

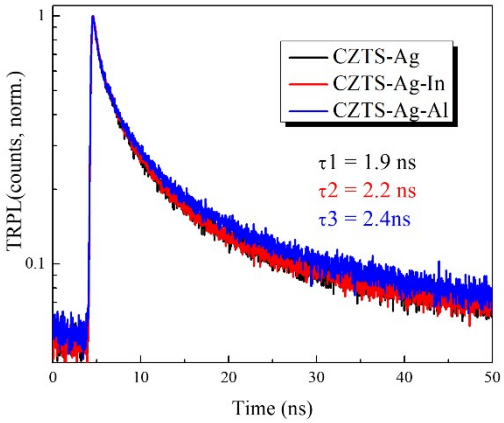

Fig. S8. Time-resolved photoluminescence decay at 532 nm excitation wavelength for CZTS devices with different interface doping.

Table S2. Summary of the results of band alignment for CZTS devices with different doping

Device	Average V_{bb} [eV± 0.01eV]	VBM-CdS [eV]	VBM-CZTS [eV]	VBO [eV± 0.01eV]	E_g-CdS [eV]	E_g-CZTS [eV]	CBO [eV± 0.01eV]
CZTS/CdS	0.15	-1.38	-0.15	-1.08	2.41	1.50	-0.14
CZTS-Ag/CdS	0.08	-1.48	-0.41	-0.99	2.41	1.50	-0.08
CZTS-Ag/CdS-In doping	0.21	-1.62	-0.37	-1.04	2.41	1.50	-0.13
CZTS-Ag/CdS-Al doping	0.22	-1.58	-0.41	-0.95	2.41	1.50	-0.05

Table S3. Device characteristics of CAZTS solar cells with different annealing temperatures (250−340 °C with 8 min) for In-doping.

Devices-In-8 min	PCE [%]	V_{OC} [mV]	FF [%]	J_{SC} [mA/cm^2]	E_g [eV]
Device-250	7.8	676	64	18.2	1.50
Device-280	9.2	708	68	19.1	1.50
Device-310	8.4	697	63	19.2	1.50
Device-340	7.4	645	59	19.5	1.50

Table S4. Device characteristics of CAZTS solar cells with different annealing times (1−15 min at 280 °C) for In-doping.

Devices-In-280	PCE [%]	V_{OC} [mV]	FF [%]	J_{SC} [mA/cm^2]	E_g [eV]
Device-1	7.1	676	61	17.3	1.50
Device-5	10.6	722	69	21.0	1.50
Device-10	9.2	703	67	19.2	1.50
Device-15	8.8	696	65	19.5	1.50

Table S5. Device characteristics of CAZTS solar cells with different annealing temperatures (250−340 °C with 8 min) for Al-doping.

Devices-Al-8 min	PCE [%]	V_{OC} [mV]	FF [%]	J_{SC} [mA/cm^2]	E_g [eV]
Device-250	9.1	703	66	19.6	1.50
Device-280	9.4	714	68	19.4	1.50
Device-310	9.3	704	67	19.7	1.50
Device-340	8.2	667	64	19.2	1.50

Table S6. Device characteristics of CAZTS solar cells with different annealing times (1−15 min at 280 °C) for Al-doping.

Devices-Al-280	PCE [%]	V_{OC} [mV]	FF [%]	J_{SC} [mA/cm^2]	E_g [eV]
Device-1	7.4	671	62	17.7	1.50
Device-5	9.2	704	66	19.8	1.50
Device-10	10.4	737	69	20.1	1.50
Device-15	9.1	711	66	19.5	1.50

Table S7. Summary of the results derived from C–V, DLCP and AS measurements for CZTS devices with different doping.

Device	N_{CV} [cm^{-3}]	N_{DLCP} [cm^{-3}]	Interface states (relative values) N_{cv}- N_{DLCP}	Defect density AS [cm^{-3}]	Carrier density AS [cm^{-3}]
CZTS	3.81×10^{16}	3.37×10^{16}	4.4×10^{15}	3.64×10^{16}	1.48×10^{16}
CZTS-Ag	2.14×10^{16}	1.98×10^{16}	1.6×10^{15}	1.73×10^{16}	5.5×10^{15}
CZTS-Ag-In	3.43×10^{16}	2.98×10^{16}	4.5×10^{15}	2.11×10^{16}	2.62×10^{16}
CZTS-Ag-Al	2.86×10^{16}	2.69×10^{16}	1.7×10^{15}	1.65×10^{16}	1.34×10^{16}

Table S8. Summary of device characteristics for CZTS solar cells with best efficiency.

Devices	η (%)	V_{OC} (mV)	FF (%)	J_{SC} (mA/cm^2)	Eg (eV)
Device-1 CZTS	6.4	640	59	16.9	1.50
Device-2 CZTS-Ag	7.6	671	64	17.5	1.50
Device-3 CZTS-Ag-In	10.6	722	69	21.0	1.50
Device-4 CZTS-Ag-Al	10.4	737	69	20.1	1.50
Device-5 CZTS-Ag-In-MgF_2	10.7	726	69	21.1	1.50
Devcie-6 CZTS-Ag-Al-MgF_2	11.2	734	71	21.2	1.50
Device-7 CZTS-Ag-In-AZO	10.4	708	67	22.1	1.50
Device-8 CZTS-Ag-Al-AZO	10.7	713	67	22.3	1.50

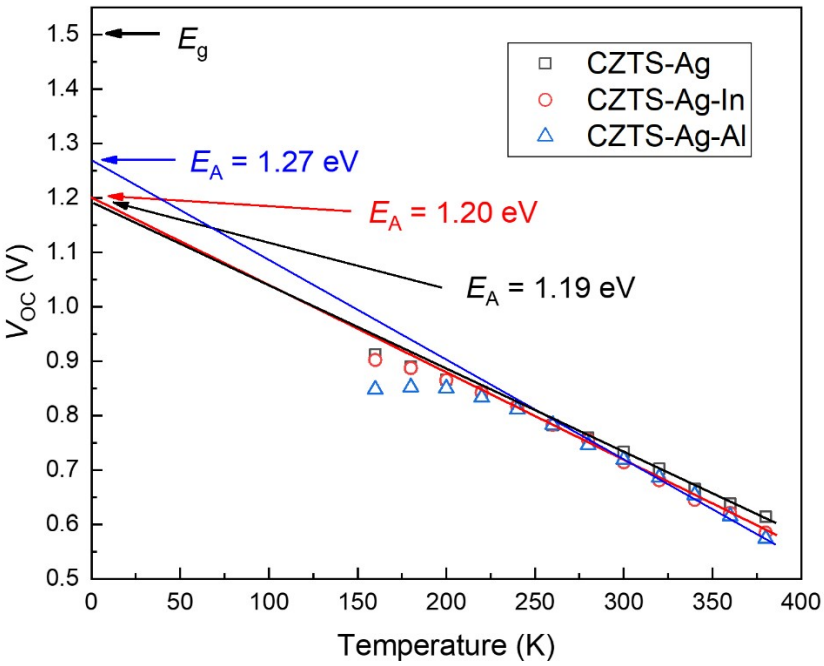

Fig. S9 Temprature-dependent open circuit measurement for CZTS devices with different doping. The activation energy (E_A) can be obtained by extrapolating the V_{OC} to a temperature of 0 K. E_g shows the bandgap of CZTS.

Dark J-V curves

The junction-dependent electrical behavior for Ag-based CZTS devices with different doping were systematically investigated and the dark J-V curves with obvious rectifying characteristics are shown in Fig. S10a. The corresponding shunt conductance G (Fig. S10b), series resistance R (Fig. S10c), diode ideality factor A (Fig. S10c), and reverse saturation current density J_0 (Fig. S10d) were obtained according to the general single exponential diode equation: [1, 2]

$$J = J_0 \exp\left[\frac{q}{AkT}(V - RJ)\right] + GV - J_L$$

For Ag-based CZTS devices with different doping (without, with In and Al doping), the diode ideality factor A values are almost same (1.57, 1.54 and 1.45, respectively), indicating a good p-n junction quality. However, for CAZTS device with Al doping,

the shunt conductance G value and reverse saturation current density J_0 are only 0.017 mS/cm^2 and 7.1×10^{-8} A/cm^2, which is obviously lower than those of the devices without and with In doping. Because of better interface band alignment for device after Al doping, therefore a smaller reverse saturation current density can be achieved indicating better unilateral conductivity of the diode and closer to the ideal transistor.

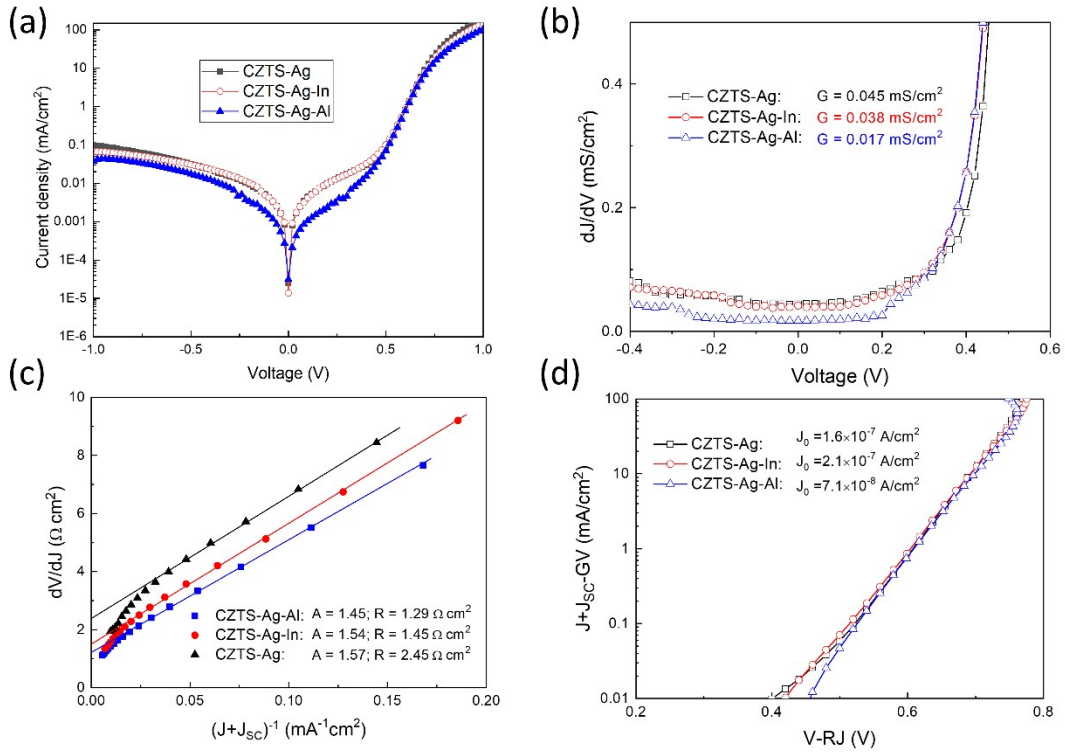

Fig. S10 Electrical behaviors of the devices (CZTS-Ag, CZTS-Ag-In, and CZTS-Ag-Al): a) Dark J-V curves; b) Shunt conductance G characterization; c) Series resistance R and ideality factor A characterization; d) Reverse saturation current density J_0 characterization.

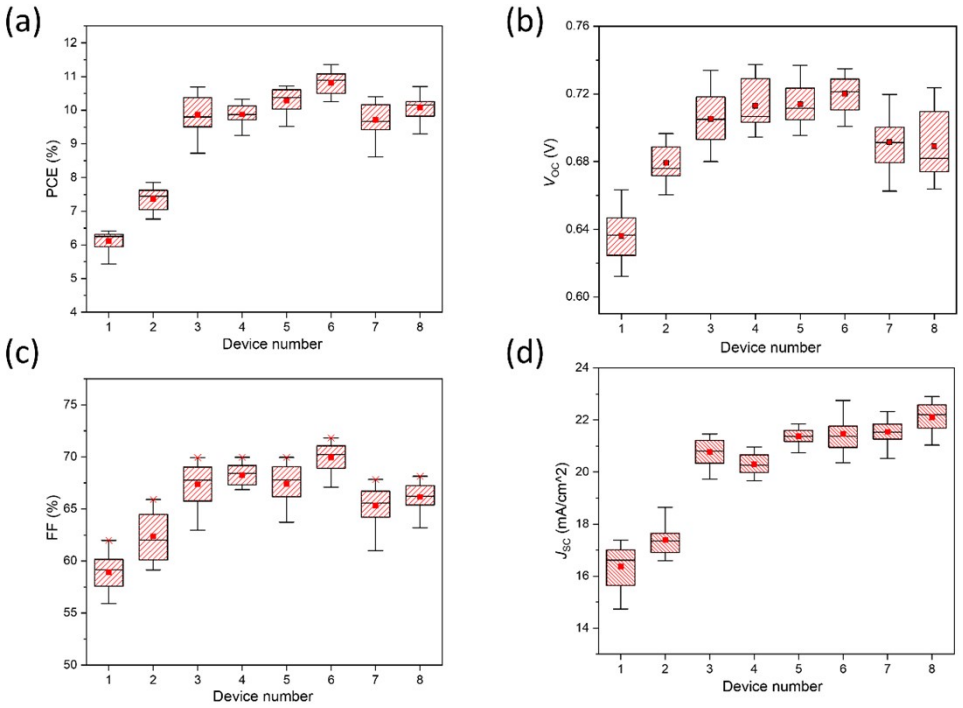

Fig. S11 The box-plot diagrams of statistical data (from 16 devices) for JV parameters from devices with different interface doping. The device number 1-8 represents pure CZTS, CZTS-Ag, CZTS-Ag-In, CZTS-Ag-Al, CZTS-Ag-In-MgF_2, CZTS-Ag-Al-MgF_2, CZTS-Ag-In-AZO, CZTS-Ag-Al-AZO, respectively.

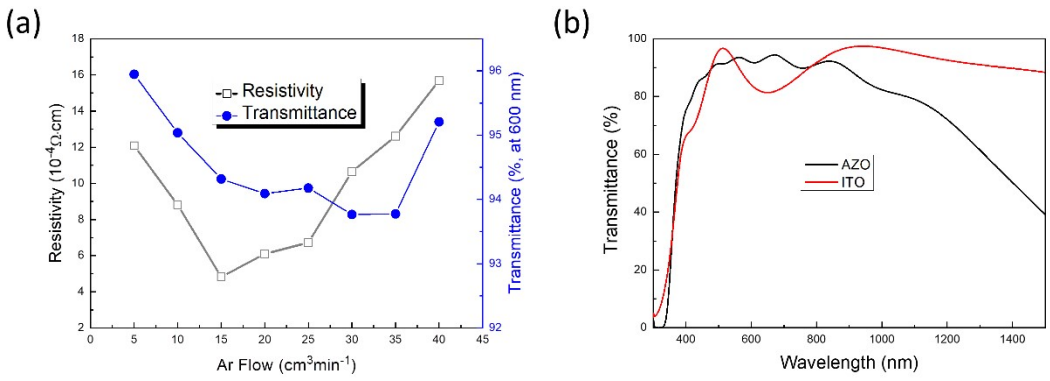

Fig. S12 a) the resistivity and transmittance (at 600 nm) of AZO thin films with different Ar flow; b) the transmittance of ITO and AZO thin films with different wavelength.

References:

1. J. R. Sites and P. H. Mauk, *Solar Cells*, 1989, **27**, 411-417.
2. S. S. Hegedus and W. N. Shafarman, *Progress in Photovoltaics: Research and Applications*, 2004, **12**, 155-176.